





Design of a Linear Time-Varying Model Predictive Control Energy Regulator for Grid-Tied VSCs

Joan-Marc Rodriguez-Bernuz , *Member, IEEE*, Ian McInerney , *Member, IEEE*,
Adrià Junyent-Ferré , *Senior Member, IEEE*, and Eric C. Kerrigan , *Senior Member, IEEE*

Abstract—This article presents an energy regulator based on a Model Predictive Control (MPC) algorithm for a Voltage Source Converter (VSC). The MPC is formulated to optimise the converter performance according to the weights defined in an objective function that trades off additional features, such as current harmonic distortion, reactive power tracking and DC bus voltage oscillation. Differently from most approaches found in the research literature, the MPC proposed here considers the coupling dynamics between the AC and DC sides of the VSC. This study is focused on the example case of a single-phase VSC, which presents a nonlinear relationship between its AC and DC sides and a sustained double-line frequency power disturbance in its DC bus. To reduce the burden of the MPC, the controller is formulated to benefit from the slow energy dynamics of the system. Thus, the cascaded structure typically used in the control of VSCs is kept and the MPC is set as an energy regulator at a reduced sampling frequency while the current control relies on a fast inner controller. The computational burden of the algorithm is further reduced by using a linear time-varying approximation. The controller is presented in detail and experimental validation showing the performance of the algorithm is provided.

Index Terms—Energy regulator, linear time-varying systems, model predictive control, power converter.

I. INTRODUCTION

THE use of power electronic converters to interface loads and generation units to the electrical grid has become more prominent over the past decades and it is foreseen that this trend will continue in the near future. This will require cost-effective power converters that can withstand disturbances, ensure power quality and operate safely within their physical limits. Some of

these requirements can be addressed through the design of controllers for the converter. While well-known controller structures based on linear regulators are predominant in industrial practice, advanced techniques based on Model Predictive Control (MPC) for high power applications are gaining momentum in recent years [1], [2]. The success of MPC is found in its capability to define the control action as an optimization problem, which estimates the future behaviour of the system based on the system information at the current time. MPC can then be used to improve the performance achieved with conventional controllers, since different system features, such as dynamic response or efficiency, amongst others, can be optimised and traded-off while input and output system constraints can be included in the control algorithm. These features provide interesting advantages for the utilisation of the converter hardware resources, allowing a closer operation to its design limits [3], [4]. Typically, the calculation of the MPC solution is comparatively harder than the calculation of a conventional linear controller. However, the development of techniques to simplify the solution of the optimisation problem and the development of more powerful hardware platforms that can perform complex computations creates an opportunity to consider advanced control techniques, such as MPC, for real-time control of power electronics.

Most of the prior work in the literature on MPC for power electronic converters consider predictive algorithms that optimise the converter switching patterns and perform basic reference tracking [5]. The main drawbacks of the most basic implementation of this idea, the Finite Control Set (FCS)-MPC, are the variable switching frequency and the fact that its computational cost grows exponentially with the prediction horizon [2], [6]. Different improved formulations can be found in the literature that overcome these limitations achieving constant modulation patterns and/or improved harmonic distortion (e.g. [5], [7], [8]). A different family of techniques, known as indirect MPC strategies, combine the predictive algorithm with an independent modulation block [5]. First, the use of hybrid models that combined explicit-MPC and Pulse Width Modulation (PWM) were proposed (e.g. [9], [10]). These techniques were found difficult to scale to complex converter topologies due to the large memory requirements and a large amount of off-line calculations. The decoupling of the predictive algorithm and the modulation stage also lead to defining the MPC as a conventional optimization problem, generally simplified as a Quadratic Programming (QP) problem [5]. Despite the local improvements that most MPC strategies provide on the regulation of the current and/or the

Manuscript received March 13, 2020; revised September 15, 2020 and January 27, 2021; accepted February 3, 2021. Date of publication February 18, 2021; date of current version May 21, 2021. This work was supported in part by the EPSRC under the Project EP/R030235/1 “RENGA: Resilient Electricity Networks for a Productive Grid Architecture” and in part by the EPSRC Centre for Doctoral Training in High Performance Embedded and Distributed Systems (HiPEDS, Grant Reference EP/L016796/1). Paper no. TEC-00260-2020. (*Corresponding author: Joan Marc Rodriguez-Bernuz.*)

Joan-Marc Rodriguez-Bernuz, Ian McInerney, and Adrià Junyent-Ferré are with the Department of Electrical and Electronic Engineering, Imperial College London, South Kensington Campus, London SW7 2AZ, U.K. (e-mail: j.rodriquez15@imperial.ac.uk; i.mcinerney17@imperial.ac.uk; adria.junyent-ferre@imperial.ac.uk).

Eric C. Kerrigan is with the Department of Electrical and Electronic Engineering, Imperial College London, London SW7 2AZ, U.K. and also with the Department of Aeronautics, Imperial College London, London SW7 2AZ, U.K. (e-mail: e.kerrigan@imperial.ac.uk).

Color versions of one or more figures in this article are available at <https://doi.org/10.1109/TEC.2021.3060319>.

Digital Object Identifier 10.1109/TEC.2021.3060319

optimisation of the switching stage of the converter [5], [11], [12], the regulation of the energy stored within the DC bus of the converter is not addressed by the predictive algorithm. In most cases, the regulation of the converter energy is achieved using a conventional linear regulator, often a slow Proportional-Integral (PI) controller. Consequently, the overall system performance is still influenced by the low bandwidth of this controller and may present poor dynamic response and overshoot [13]. An attempt to tackle this issue is found in [14], which explored the design of a predictive controller considering the instantaneous power of the converter (which was taken as constant as in balanced three-phase systems). However, the methodology may not be suitable for single-phase or unbalanced three-phase systems, where the power would contain a double line frequency term. As a workaround, [13] proposed a cascade-free FCS-MPC combined with an averaging filter to deal with the nonlinear dynamics of the power exchanged in a single-phase neutral-point clamped converter. Nevertheless, this filtering inherently restricts the bandwidth of the energy regulation. A different approach to deal with the converter energy regulation is presented in [15], [16], where a predictive controller is used to pre-compensate the energy control reference of the power converter by considering a Reference Governor (RG) structure which achieves improved closed-loop response compared to conventional controllers. Following a similar idea, [17] explored the design of a predictive reference generator based on a nonlinear model of the system, although the real-time implementation of nonlinear optimisation was not solved.

In this paper, the predictive algorithm is formulated as an outer energy regulator which takes into account the average energy dynamics of the Voltage Source Converter (VSC). Differently from MPC strategies that address the predictive algorithm from the modulation stage, e.g. [7], [13], the algorithm presented here relies on a cascaded structure with a PWM modulator. Since the instantaneous nonlinear power equality is implicitly included in the MPC formulation, optimal transient and steady-state performance is ensured; outperforming other strategies where the converter energy regulation is restricted (e.g. [13]). The combination of MPC with PWM can potentially lead to a reduction of the computational effort since the integer states of the switching stage are simplified by using a reduced equivalent model. However, the use of a PWM also leads to potential performance degradation from the modulation point of view, since the optimisation of switching stage brought by direct MPC is lost. Although the optimisation of the modulation stage is not addressed here, a comparison of the modulation performance between direct MPC algorithms and conventional strategies can be found in [5], [18].

In this paper, the MPC energy regulator is designed to account for a long predictive horizon (e.g. 10 ms) in order to optimise the closed-loop performance of all converter states. Furthermore, the formulation of MPC as a classic optimisation problem ensures that the addition of constraints to guarantee that converter physical limitations are not exceeded and other additional features, such as harmonic restrictions, can be added with ease. The formulation of MPC problems considering the nonlinear system equations are generally addressed by performing a direct linearisation to turn the system into a Linear Time-Invariant (LTI) one [2], [5]. While this strategy is feasible

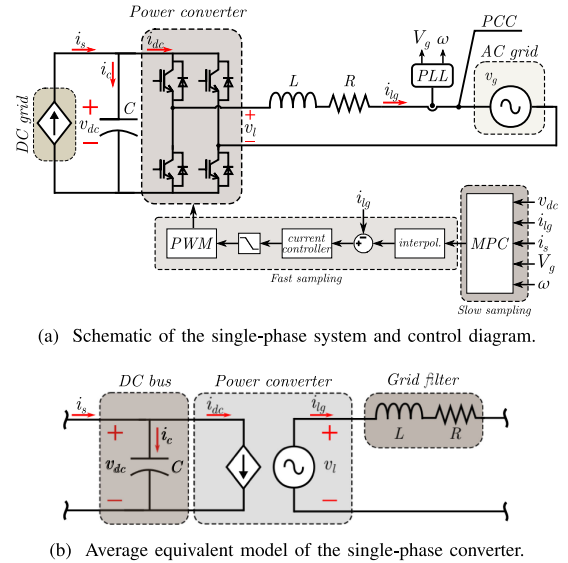


Fig. 1. Diagram of the single-phase converter.

for short prediction horizons and reduced time-steps, the highly nonlinear trajectories of the single-phase system detracts from applying this approach over a long prediction horizon. This paper presents a novel approach based on a Linear Time-Varying (LTV) formulation. Here, the system dynamics over the receding horizon are divided between foreseen steady-state nonlinear periodic trajectories and a complementary LTI system is used to formulate the MPC problem. Furthermore, the MPC is designed following a hierarchical multi-rate structure; cascading the predictive energy regulator with an inner current controller. This approach permits one to significantly reduce the sampling frequency of the MPC for its real-time implementation when compared to other MPC approaches (e.g. [7], [13]). Additionally, the design of a high-bandwidth inner regulator brings robustness in front of fast current dynamic changes.

The LTV-MPC algorithm is presented in the example case of a single-phase two-level converter given the particular challenge arising from the nonlinear relationship between its AC and DC sides, which creates a double-line frequency power disturbance. However, the methodology can be easily extrapolated to other complex converters, being of special interest in complex power converters with several control degrees of freedom as shown in [19].

II. SYSTEM MODELLING

The converter under analysis is an H-bridge single-phase AC/DC converter, i.e. two legs and two switching devices per leg connected to a large capacitor (see Fig. 1(a)). The AC side is interfaced with the grid by means of a coupling filter. For simplification purposes, the AC grid is considered as a stiff voltage source and the DC grid is modelled as a current source. The semiconductor devices in power electronics converters are operated as switches that can be either closed or open. Consequently, the converters behave as nonlinear systems operated in a discrete fashion. However, the system can be reduced to a conventional equivalent average model, as shown in Fig. 1(b), given that the commutation of the switching devices lies at a much higher

frequency than the energy dynamics to be controlled by the MPC [20]. The DC side of the converter is then modelled as a controlled current source and the AC side is approximated as a controlled voltage source.

Considering that the converter losses are negligible, the power balance within the converter is defined as

$$v_l i_{lg} = v_{dc} i_{dc}. \quad (1)$$

Next, the analysis of the AC side current of the equivalent system shown in Fig. 1(b) yields

$$\frac{d}{dt} i_{lg} = \frac{1}{L} (v_l - v_g - R i_{lg}). \quad (2)$$

The voltage of the DC bus is a function of the current flowing through its capacitance, which gives

$$\frac{d}{dt} v_{dc} = \frac{1}{C} i_c = \frac{1}{C} \left(i_s - \frac{v_l i_{lg}}{v_{dc}} \right). \quad (3)$$

The resulting state-space representation of the single-phase converter accounts for a single control variable v_l , which is the voltage modulated by the converter, and two state variables: the DC bus voltage v_{dc} and the AC grid current i_{lg} . The incoming current from the DC side i_s and the AC grid voltage v_g are considered to be external disturbances. The system equations can be written in matrix form as

$$\begin{aligned} \frac{d}{dt} \begin{bmatrix} v_{dc} \\ i_{lg} \end{bmatrix} &= \begin{bmatrix} 0 & 0 \\ 0 & -\frac{R}{L} \end{bmatrix} \begin{bmatrix} v_{dc} \\ i_{lg} \end{bmatrix} + \begin{bmatrix} \frac{-i_{lg}}{C v_{dc}} \\ \frac{1}{L} \end{bmatrix} v_l \\ &+ \begin{bmatrix} \frac{1}{C} & 0 \\ 0 & -\frac{1}{L} \end{bmatrix} \begin{bmatrix} i_s \\ v_g \end{bmatrix}. \end{aligned} \quad (4)$$

Note that the single-phase power contains an oscillating component at double line frequency as a result of the power balance equation of the converter.

III. PRELIMINARY NONLINEAR MPC

This section provides a comparison between the nonlinear MPC and the LTV approximation discussed in Section IV. The overall control structure is illustrated in Fig. 1(a). For illustrative purposes, a simplified version of the energy regulator is presented here in order to analyse the performance of the algorithm for the nonlinear case. The preliminary nonlinear MPC is designed to trade off the DC bus voltage oscillation and system efficiency, i.e. root mean square (RMS) of the grid current, as in [17]. The objective function to minimise is

$$\begin{aligned} \min_{v_l, i_{lg}, v_{dc}} & \frac{1}{2} \sum_{k=1}^{N-1} \underbrace{(v_{dc[k]} - v_{dc}^*)^\top \mathcal{S} (v_{dc[k]} - v_{dc}^*)}_{\text{term 1}} \\ & + \frac{1}{2} \underbrace{(v_{dc[N]} - v_{dc}^*)^\top \mathcal{S}_N (v_{dc[N]} - v_{dc}^*)}_{\text{term 2}} \\ & + \frac{1}{2} \underbrace{\sum_{k=1}^N i_{lg[k]}^\top \mathcal{R} i_{lg[k]}}_{\text{term 3}} + \frac{1}{2} \underbrace{\sum_{k=0}^{N-1} v_{l[k]}^\top \mathcal{U} v_{l[k]}}_{\text{term 4}} \end{aligned} \quad (5a)$$

TABLE I
PARAMETERS OF THE EXPERIMENTAL TEST-BENCH

| MPC test-bench | | Triphase cabinet | |
|----------------|---------------------|------------------|----------------------|
| Parameter | Value | Parameter | Value |
| P_N | 450 W | P_N | 15 kVa |
| V_g | 50 V _{RMS} | V_z^{ac} | 380 V _{RMS} |
| V_{DC} | 110 V | V_z^{dc} | 480 V |
| R_{DC} | 50 Ω | L_z | 2 mH |
| L | 0.101 mH | C_z | 3 mF |
| R | 0.06 Ω | R_e | 0.2 Ω |
| C | 0.89 mF | L_e | 2.3 mH |

where \mathcal{R} , \mathcal{S} , \mathcal{U} are weights, and \mathcal{S}_N is a terminal weight. A discrete-time sample is denoted by k and N is the number of samples of the receding horizon. Term 1 stabilises and reduces the DC bus oscillation around v_{dc}^* , term 2 is the last sample of the horizon, term 3 accounts for the minimisation of the AC current and term 4 minimises the control action v_l . Interestingly, larger values of \mathcal{S} would cause the controller to minimise the DC bus oscillation by injecting larger AC grid current harmonics. In contrast, a larger \mathcal{R} would reduce the AC grid RMS current at the expense of increasing the DC bus oscillation. Because of this negative correlation, it is imposed that $\mathcal{S} + \mathcal{R} = 1$. Additionally, it is desired that the control action has a negligible impact on the steady-state performance; thus, a very low weight is assigned to this parameter ($\mathcal{U} \sim 10^{-3}$).

The system equations, input and output boundaries are included in the optimisation as the following constraints:

$$discrete\{(4)\} \quad k = 0, \dots, N-1 \quad (5b)$$

$$\check{v}_{dc} \leq v_{dc[k]} \leq \hat{v}_{dc} \quad k = 1, \dots, N \quad (5c)$$

$$\check{i}_{lg} \leq i_{lg[k]} \leq \hat{i}_{lg} \quad k = 1, \dots, N \quad (5d)$$

$$\check{v}_l \leq v_{l[k]} \leq \hat{v}_l \quad k = 0, \dots, N-1 \quad (5e)$$

where Δt is the sampling period. The discrete approximation of the plant is given by (5b) — the term $discrete\{\cdot\}$ refers to the equivalent discrete approximation of the designated equation — and is based on a second order truncated Taylor series [21], sampled at frequency f_{mpc} . The variables $\{\hat{i}_{lg}, \check{i}_{lg}\}$ are the upper and lower bounds of i_{lg} , $\{\hat{v}_{dc}, \check{v}_{dc}\}$ are the operating limits of the bus voltage and $\{\hat{v}_l, \check{v}_l\}$ are bounds of the control input. The maximum instantaneous AC current is bounded by (5d), while (5c) bounds the values that the DC bus voltage can take and (5e) bounds the control voltage that can be applied. Note that $|\check{v}_l, \hat{v}_l| \leq \check{v}_{dc}$.

A. Evaluation & Comparison

The LTV-MPC algorithm described in Section V has been adapted to match the algorithm described in Section III. The tuning parameters are summarised in Table II. First, Fig. 2 shows the trajectories of the states for both approaches. The tuning weight \mathcal{S} is chosen as 0.7 so that the algorithm prioritises the reduction of the DC bus voltage oscillation by injecting a large harmonic content into the AC current. Nevertheless, it can be

TABLE II
TUNING PARAMETERS OF THE PREDICTIVE ALGORITHM

| MPC algorithm | | Notch Filter | |
|--|---------|------------------|--------------|
| T_h | 10 ms | a_1, b_1 | 0.88, 1.00 |
| f_s | 1 kHz | a_2, b_2 | -3.37, -3.58 |
| N_Q | 10 | a_3, b_3 | 4.98, 4.97 |
| N_K | 5 | a_4, b_4 | -3.37, -3.16 |
| \mathcal{W} | 3 | a_5, b_5 | 0.88, 0.78 |
| $\hat{v}_{lg}, \hat{v}_{ig}$ | -15, 15 | OSQP parameters | |
| $\hat{v}_{dc}, \hat{v}_{dc}$ | 90, 140 | $max. iter$ | 150 |
| \hat{v}_l, \hat{v}_l | -90, 90 | $solve time$ | 0.9 ms |
| Current Controller | | ϵ_{abs} | 0.01 |
| $H_\infty = \begin{bmatrix} 11.87s^2 + 18.78s & 6.91 \\ 1.00s^2 + 0.86s & -0.13 \end{bmatrix}$ | | ϵ_{ref} | 0.01 |
| | | ρ | 0.0035 |

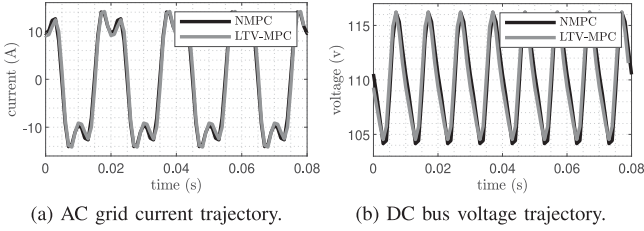


Fig. 2. Comparison of the LTV and NL models over time ($S = 0.7$).

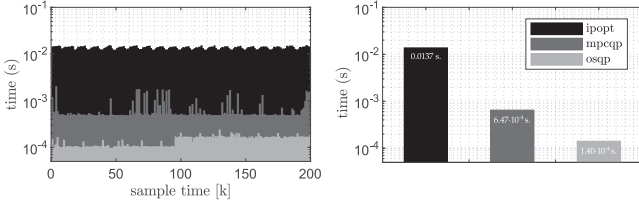


Fig. 3. Computation time required by solvers (tuning factor $S = 0.2$). This comparison has been performed running the algorithm on a 3.5 GHz Intel Xeon.

seen that the system trajectories are quite similar, indicating that the LTV simplification does not introduce a large modelling error in the MPC algorithm.

Furthermore, the time-to-solution of the algorithm over 100 samples is shown in Fig. 3. Despite the simplicity of this regulator compared to the full algorithm described in Section V, the computational requirements of the nonlinear model is too high for its implementation and the computation time with the LTV approximation is around 2 orders of magnitude faster.

IV. LTV-MPC APPROXIMATION

This section describes the approach followed to relax the computational burden of the nonlinear MPC algorithm by applying a linear time-varying (LTV) approximation. This approach permits one to retain the main nonlinear dynamics of the converter while the predictive algorithm can be formulated on a linear system, thereby decreasing the computational burden of solving the optimal control problem. The performance obtained with the nonlinear model and the LTV approximation is shown in Fig. 2. The LTV model is based on decoupling the system dynamics in two differentiated levels. For convenience, they are referred to as high-level and low-level dynamics. Similarly to the

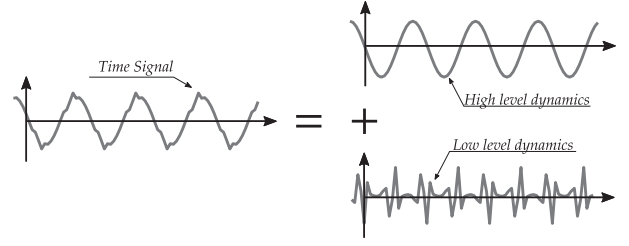


Fig. 4. Illustration of the time signal decomposition.

small-signal analysis in linear time-invariant (LTI) systems [20], the high-level trajectory determines the nonlinear behaviour of the system and the low-level describes small signal deviations around the main trajectory points. However, instead of considering a DC quiescent point, the linearisation is performed over a time-varying trajectory. The signal decomposition is illustrated in Fig. 4.

A. General LTV Modeling

The generic nonlinear system

$$\frac{d}{dt}x(t) = f(x(t), u(t), w(t)) \quad (6)$$

where $x(t)$ is a generic state, $u(t)$ is the control input and $w(t)$ a disturbance, is considered here to introduce the derivation of the LTV model. This system can be regarded as a generalisation of the converter plant in (4). The generalisation of the LTV approximation uses the system variables

$$x(t) = \tilde{x}(t) + \delta x(t) \quad (7)$$

$$u(t) = \tilde{u}(t) + \delta u(t) \quad (8)$$

$$w(t) = \tilde{w}(t) + \delta w(t) \quad (9)$$

where the variables designated with the accent ($\tilde{\cdot}$) describe steady periodic trajectories that vary over time and the symbol δ designates disturbances around them.

The linearisation of the system described in (6) around the steady trajectories $\{\tilde{x}(t), \tilde{u}(t), \tilde{w}(t)\}$ yields

$$\begin{aligned} \frac{d}{dt}x(t) &\approx \frac{d}{dt}\tilde{x}(t) + \frac{d}{dt}\delta x(t) = f(\tilde{x}(t), \tilde{u}(t), \tilde{w}(t)) \\ &+ \frac{\partial f(\tilde{x}(t), \tilde{u}(t), \tilde{w}(t))}{\partial x} \delta x(t) \\ &+ \frac{\partial f(\tilde{x}(t), \tilde{u}(t), \tilde{w}(t))}{\partial u} \delta u(t) \\ &+ \frac{\partial f(\tilde{x}(t), \tilde{u}(t), \tilde{w}(t))}{\partial w} \delta w(t), \end{aligned} \quad (10)$$

where

$$\frac{d}{dt}\tilde{x}(t) = f(\tilde{x}(t), \tilde{u}(t), \tilde{w}(t)) \quad (11)$$

retains the nonlinear behaviour of the system and is obtained based on the steady-state trajectories of the system at specific operating points. The resulting state-space model used to define

the optimal control problem can be expressed as

$$\frac{d}{dt}\delta x(t) = \mathcal{A}(t)\delta x(t) + \mathcal{B}(t)\delta u(t) + \mathcal{E}(t)\delta w(t), \quad (12)$$

where

$$\mathcal{A}(t) = \frac{\partial f(\tilde{x}(t), \tilde{u}(t), \tilde{w}(t))}{\partial x}, \quad (13)$$

$$\mathcal{B}(t) = \frac{\partial f(\tilde{x}(t), \tilde{u}(t), \tilde{w}(t))}{\partial u}, \quad (14)$$

$$\mathcal{E}(t) = \frac{\partial f(\tilde{x}(t), \tilde{u}(t), \tilde{w}(t))}{\partial w}. \quad (15)$$

The derivation of the steady-state trajectories and the resulting linear state-space model for the example case under analysis are provided, respectively, in Appendices A and B. The LTV solution is evaluated at time t_k over the receding control horizon such that the resulting state-space can be expressed as

$$\frac{d}{dt}\delta x(t_k) = \mathcal{A}(t_k)\delta x(t_k) + \mathcal{B}(t_k)\delta u(t_k). \quad (16)$$

where $k = 0, \dots, N$ represent the sampling instant at which the system is evaluated. For each particular sampling point k of the prediction horizon, the system can then be generically expressed in the discrete domain as

$$\delta x_{[k+1]} = A_{[k]}\delta x_{[k]} + B_{[k]}\delta u_{[k]}, \quad (17)$$

where $A_{[k]}$ and $B_{[k]}$ are equivalent discrete-time matrices for the time instances t_k at which \mathcal{A} and \mathcal{B} are evaluated.

V. LTV-MPC CONTROLLER

This section introduces a detailed description on the design of the LTV-MPC algorithm. The regulator follows the form presented in Section III. Reactive power tracking and current harmonic constraints are also incorporated in the algorithm. Note that the controller is designed considering the LTV approximation described in Section IV.

A. Reactive Power Formulation

The reactive power is modelled in the temporal domain as the average product over \mathcal{N}_Q samples of the grid current i_{lg} and an orthogonal vector in quadrature with the grid voltage v_{Qg} . Although this definition of reactive power might be inaccurate in the presence of harmonic components in the AC grid [22], it was found to be an acceptable approximation at a reduced computational cost. Note that the apparent power of the system has an oscillation at 100 Hz, which permits one to choose the length of the averaging filter as half of the grid frequency. The reactive power filter is designed to not only consider \mathcal{N}_P measured samples, but also to include data from the receding horizon. Therefore, the reactive power is defined as a trade-off between past and prediction points as

$$Q = \frac{1}{\mathcal{N}_Q} \sum_{k=-\mathcal{N}_P}^{\mathcal{N}_Q-\mathcal{N}_P} i_{lg[k]} \times v_{Qg[k]}. \quad (18)$$

The reactive power expression can be rewritten considering the LTV transformation presented in Section IV. The reactive

power can be split between past and prediction samples as

$$Q = \mathcal{K} + \frac{1}{\mathcal{N}_Q} \sum_{k=1}^{\mathcal{N}_Q-\mathcal{N}_P} i_{lg[k]} \times v_{Qg[k]} = \tilde{Q} + \delta Q, \quad (19)$$

where

$$\mathcal{K} = \frac{1}{\mathcal{N}_Q} \sum_{k=-\mathcal{N}_P}^0 i_{lg[k]} \times v_{Qg[k]}, \quad (20)$$

$$\tilde{Q} = \mathcal{K} + \frac{1}{\mathcal{N}_Q} \sum_{k=1}^{\mathcal{N}_Q-\mathcal{N}_P} \tilde{i}_{lg[k]} \times v_{Qg[k]}, \quad (21)$$

$$\delta Q = \frac{1}{\mathcal{N}_Q} \sum_{k=1}^{\mathcal{N}_Q-\mathcal{N}_P} \delta i_{lg[k]} \times v_{Qg[k]}, \quad (22)$$

\mathcal{K} is a constant term that is updated at each sampling instant as new values of current and voltage are obtained, \tilde{Q} is calculated from past data and steady-state trajectories and δQ describes the low-level system dynamics.

B. Harmonic Constraint

In [23], the output current spectrum of the converter is limited by adding a weighted peak filter into the objective function of an FCS-MPC algorithm. The use of an IIR filter is also introduced in [8] to estimate the spectrum of the switching frequency obtained with a predictive controller. A similar approach is adopted here and the harmonic components of the current are obtained by applying an IIR notch filter in order to exclude the fundamental component of grid frequency. The output of the filter can then be restricted and included in the optimisation as a constraint. Note that the filter must be carefully designed, since spectrum leakage might provide a gain at the fundamental frequency, which would change the dynamic response of the system. In order to avoid infeasibility, this constraint is also relaxed adding softening variables into the objective function. The difference equation of the notch filter implemented is as follows:

$$\begin{aligned} b_1 \cdot y[k] &= a_1 \cdot u[k] + a_2 \cdot u[k-1] + a_3 \cdot u[k-2] \\ &\dots + a_4 \cdot u[k-3] + a_5 \cdot u[k-4] - b_2 \cdot y[k-1] \\ &\dots - b_3 \cdot y[k-2] - b_4 \cdot y[k-3] - b_5 \cdot y[k-4] \end{aligned} \quad (23)$$

where k is the sampling instant, u is the input, y is the output, a_1, \dots, a_5 and b_1, \dots, b_5 are filter coefficients.

The AC current harmonic constraint is formulated considering the LTV approximation given in Section IV. Besides, this constraint is stated from the $k + 2$ sample of the prediction horizon to include the computational delay compensation of the MPC block (see Section V-F). Then, the harmonic constraint is as follows:

$$-\mathcal{T} \leq (-a_1 b_2 + a_2) \cdot \delta i_{lg[k+1]} + a_1 \cdot \delta i_{lg[k+2]} + \mathcal{C} \leq \mathcal{T} \quad (24)$$

and,

$$\begin{aligned}
\mathcal{C} = & a_1 \tilde{i}_{lg[k+2]} + a_2 \cdot \tilde{i}_{lg[k+1]} + a_3 \cdot i_{lg[k]} + a_4 \cdot i_{lg[k-1]} \\
& \dots + a_5 \cdot i_{lg[k-2]} - b_2 \cdot \tilde{y}[k+1] - b_3 \cdot \tilde{y}[k] \\
& \dots - b_4 \cdot y[k-1] - b_5 \cdot y[k-2].
\end{aligned} \tag{25}$$

where \mathcal{T} is the maximum value that the summation of all the harmonic components of the signal could have at a particular instant of time. Note that \mathcal{C} accounts for past samples and steady-state trajectory points that are invariant for the formulation of the LTV-MPC problem.

C. Objective Function

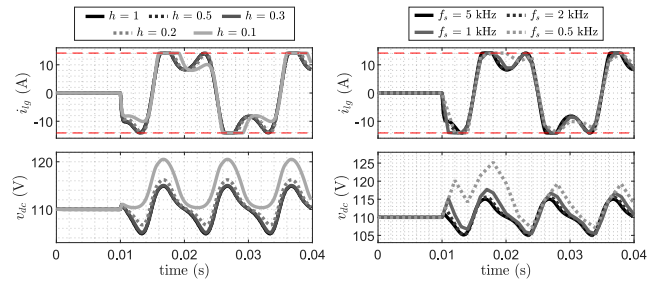
The objective function follows the form presented in (5a), although it includes the LTV approximation described in Section IV and additional terms to account for the reactive power tracking and the relaxation of the current harmonic constraints:

$$\begin{aligned}
\min_{\substack{\delta v_{dc}, \delta i_{lg} \\ \delta v_l, \delta Q \\ \lambda_1, \lambda_2}} & \frac{1}{2} (\delta v_{dc[N]} + \tilde{v}_{dc[N]} - v_{dc}^*)^\top \mathcal{S}_N (\delta v_{dc[N]} + \tilde{v}_{dc[N]} - v_{dc}^*) \\
& \underbrace{\hspace{10em}}_{\text{term 1}} \\
& + \frac{1}{2} \sum_{k=1}^{N-1} (\delta v_{dc[k]} + \tilde{v}_{dc[k]} - v_{dc}^*)^\top \mathcal{S} (\delta v_{dc[k]} + \tilde{v}_{dc[k]} - v_{dc}^*) \\
& \underbrace{\hspace{10em}}_{\text{term 2}} \\
& + \frac{1}{2} \sum_{k=1}^N (\delta i_{lg[k]} + \tilde{i}_{lg[k]} - i_{lg}^*)^\top \mathcal{R} (\delta i_{lg[k]} + \tilde{i}_{lg[k]} - i_{lg}^*) \\
& \underbrace{\hspace{10em}}_{\text{term 3}} \\
& + \frac{1}{2} \sum_{k=0}^{N-1} (\delta v_{l[k]} + \tilde{v}_{l[k]} - v_l^*)^\top \mathcal{U} (\delta v_{l[k]} + \tilde{v}_{l[k]} - v_l^*) \\
& \underbrace{\hspace{10em}}_{\text{term 4}} \\
& + \frac{1}{2} (\delta Q + \tilde{Q} - Q^*)^\top \mathcal{Y} (\delta Q + \tilde{Q} - Q^*) \\
& \underbrace{\hspace{10em}}_{\text{term 5}} \\
& + \frac{1}{2} \lambda_1 \mathcal{W} \lambda_1 + \frac{1}{2} \lambda_2 \mathcal{W} \lambda_2 \\
& \underbrace{\hspace{3em}}_{\text{term 6}} \quad \underbrace{\hspace{3em}}_{\text{term 7}}
\end{aligned} \tag{26a}$$

where δv_{dc} , δi_{lg} , δv_l , δQ , λ_1 and λ_2 are decision variables; \tilde{v}_{dc} , \tilde{i}_{lg} , \tilde{v}_l , \tilde{Q} are trajectory values; v_{dc}^* , i_{lg}^* , v_l^* , Q^* are reference set-points; and \mathcal{S}_N , \mathcal{S} , \mathcal{R} , \mathcal{U} , \mathcal{Y} and \mathcal{W} are weights. Term 1 accounts for the deviation of the last term in the prediction horizon, term 2 accounts for the reduction of the DC bus voltage ripple around reference values, term 3 weights the RMS of AC grid current, term 4 minimises the control action, term 5 accounts for the tracking of the reactive power and term 6 and 7 penalise the violation of the harmonic current constraint.

D. Constraints Definition

Similarly, the optimisation constraints are formulated using the steady-state trajectories:



(a) Effect of prediction horizon length. (b) Effect of sampling frequency.

Fig. 5. Effect of tuning parameters T_h and f_{mpc} on the system performance.

$$\text{discrete}\{(37)\} \quad k = 0, \dots, N-1 \tag{26b}$$

$$\text{discrete}\{(22)\} \quad k = 1, \dots, \mathcal{N}_Q - \mathcal{N}_P \tag{26c}$$

$$\tilde{v}_{dc} \leq \tilde{v}_{dc[k]} + \delta v_{dc[k]} \leq \hat{v}_{dc} \quad k = 1, \dots, N \tag{26d}$$

$$\tilde{i}_{lg} \leq \tilde{i}_{lg[k]} + \delta i_{lg[k]} \leq \hat{i}_{lg} \quad k = 1, \dots, N \tag{26e}$$

$$\tilde{v}_l \leq \tilde{v}_{l[k]} + \delta v_{l[k]} \leq \hat{v}_l \quad k = 0, \dots, N-1 \tag{26f}$$

$$\begin{aligned}
\lambda_1 - \mathcal{T} & \leq (-a_1 b_2 + a_2) \cdot \delta i_{lg[k+1]} \\
& + a_1 \cdot \delta i_{lg[k+2]} + \mathcal{C} \leq \mathcal{T} + \lambda_2 \quad k = 0
\end{aligned} \tag{26g}$$

where $\{\check{v}_{dc}, \hat{v}_{dc}\}$, $\{\check{i}_{lg}, \hat{i}_{lg}\}$ and $\{\check{v}_l, \hat{v}_l\}$ are the upper and lower bounds of the system states and the control variable, (26b) and (26b) are the system and reactive power models, (26c) constraints the DC bus voltage, (26e) limits the peak of the AC grid current, (26f) restricts the control action and (26g) restricts the harmonic content of the AC current.

E. Horizon Length & Sampling Frequency

The effect of different horizon lengths and sampling frequencies is shown in Fig. 5. This analysis is run considering a scenario where the converter operates at 1 pu, power factor 1, and $\mathcal{S} = 0.8$. In order to evaluate the performance of the algorithm, the trajectories are analysed under a transient excursion and in steady-state. First, Fig. 5(a) provides insight about the effect of reducing the prediction horizon while the sampling frequency is kept relatively high, e.g. 5 kHz. Note that h is a multiple of the fundamental system frequency, which determines the length of the control horizon T_h , e.g. $h = 0.5 \rightarrow T_h = 0.5 \cdot 20 \text{ ms} = 10 \text{ ms}$. Based on the information obtained in Fig. 5(a), Fig. 5(b) evaluates different sampling frequencies, fixing the horizon length as $h = 0.3$. The results indicate that $h = 0.3$ and $f_{mpc} = 1 \text{ kHz}$ provides acceptable performance.

F. Interpolation & Delay Compensation

Given the low sampling rate of the MPC algorithm, the points of the control horizon are interpolated in order to smooth the

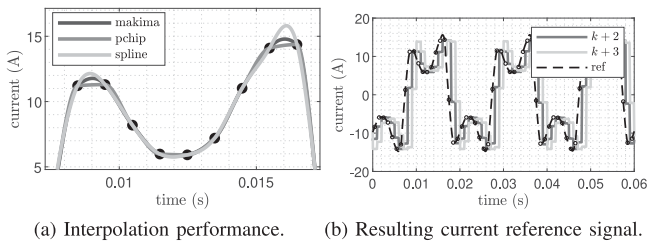


Fig. 6. Illustration of the interpolation and delay compensation performance.

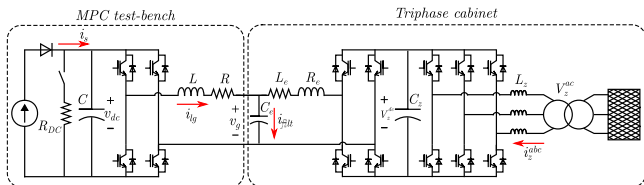


Fig. 7. Schematic of the experimental setup.

current references passed to the current controller. The interpolation function is based on the modified Akima cubic hermite (MAKIMA) function available in *Matlab* [24]. The performance of the interpolation is compared against the interpolation functions *pchip* and *spline* also available in *Matlab* [24] (see Fig. 6(a)). Note that current control references are determined considering the $k + 2$ and $k + 3$ horizon points in order to compensate for the computational delay of the MPC block. The resulting reference signal obtained with the MAKIMA function and the delay compensation is illustrated in Fig. 6(b).

VI. EXPERIMENTAL VALIDATION

The performance of the LTV-MPC algorithm was validated in an experimental platform with different weights and tuning parameters. The experimental bench consisted of a single-phase converter that interfaces a DC link with a slack single-phase AC grid. The slack AC grid was obtained by adapting a three-phase back-to-back converter, whose inverter was configured to operate as a single-phase AC grid emulator. The DC grid was achieved using a DC power source programmed to saturate the DC current at a desired level. In order to generate power step changes, a parallel resistor R_{DC} was added to consume 50 % of the platform nominal power. The system was controlled using an *Opal-RT* 5600 unit and a *Triphase* target. An illustration and schematic of the system are shown in Fig. 7 and Fig. 8, respectively. The parameter values of the setup are summarised in Table I.

The LTV-MPC controller presented in Section V was implemented in the *Opal-RT* target using the OSQP solver [25]. OSQP is a solver for convex quadratic programs based on the alternating direction method of multipliers that is written in C and interfaced with the *Opal-RT* through a Simulink S-function. The LDL factorization routine at the core of OSQP uses the sparsity pattern of the problem matrices to perform a symbolic factorization at design-time, allowing for the values in the matrices to be updated more efficiently at runtime.

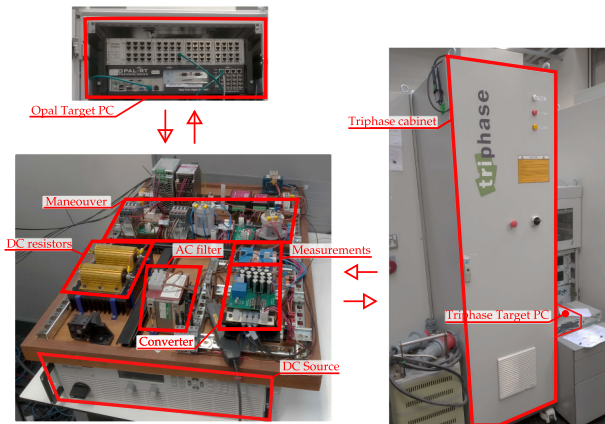


Fig. 8. Illustration of the different elements of the experimental bench.

In this work, the non-zero entries of the optimization matrices are updated with the new linearized system dynamics at every sampling instant. The solver is then warm-stated with the previous solution at each sampling instant. It was found that the computation time and number of iterations needed to solve the problem largely depended on the solver configuration parameters ϵ_{abs} , ϵ_{rel} and the step-size ρ . The parameters shown in Table II were chosen based on the observed performance, and it was found that the number of iterations required when the converter was in steady-state was 25 and the maximum solver time/iterations was not reached during any of the tests performed.

The performance of the OSQP solver was compared with *mpcqsolver* from the *Matlab* MPC Toolbox [26], which uses an active-set method based on the KWIK algorithm, and the results are shown in Fig. 3. The grid information was estimated from a Park-PLL [27] and the current regulator was based on an H_∞ [28] controller (see Table II).

The MPC algorithm was divided between two cores: core 1 was sampled at a high frequency, namely 25 kHz, and implemented the interpolating function, the current controller, the PLL and the PWM. Core 2 was sampled at a low frequency, namely 1 kHz, and implemented the MPC. The optimization algorithm was run to completion consistently below 0.5 ms in the *Opal-RT* control target. The control structure is illustrated in Fig. 1(a).

1) *Steady-State*: The steady-state performance for two different S weights is shown in Fig. 9. Both cases are compared against a PI energy regulator, whose dynamics are displayed in the background. The tuning parameters of the PI are $K_P = 0.1$ and $K_I = 1.42$. As can be seen in Fig. 9(a), low S values lead to similar trajectories as those obtained with the PI. On the other hand, the increment of S produces a large injection of harmonics in the current, which decreases the DC bus voltage oscillation. Note that this scenario is illustrative of the potential of the energy regulator but is not the control objective to inject a large quantity of current harmonics into the AC grid. Nevertheless, this controller could be used in complex converters to meet additional control goals as in [19].

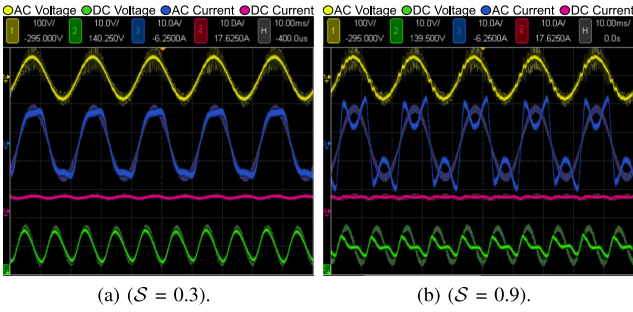


Fig. 9. Experimental steady-state system trajectories.

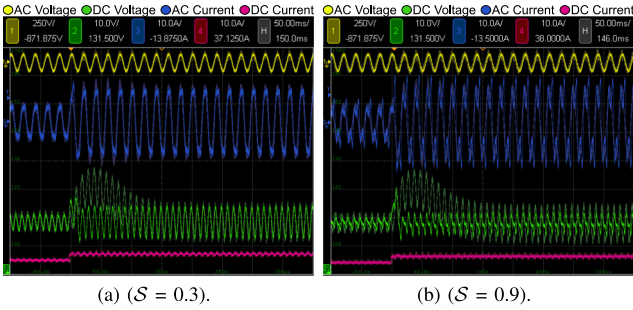


Fig. 10. Experimental transient response for a step change from 0.5 to 1 p.u.

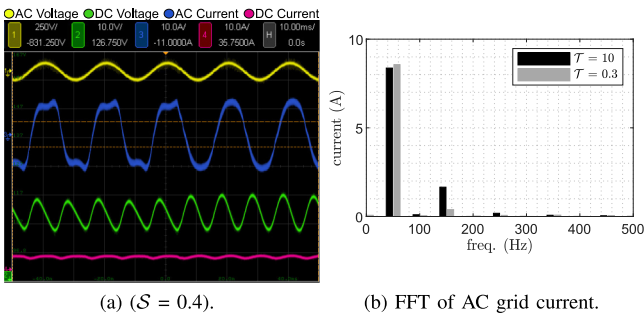


Fig. 11. Effect of tightening the harmonic constraint bounds.

2) *Transient Response*: The transient response of the system to a step-change from 0.5 to 1 p.u. is shown in Fig. 10 for weights $S = 0.3$ and 0.9. The PI trajectories are displayed in the background for comparison purposes. As can be seen, MPC achieves a faster regulation and reduced overshoot compared to PI control.

3) *Harmonic Constraint*: The capability of the algorithm to limit the harmonic content of the output current is shown in Fig. 11(a), where the harmonic bounds are tightened from $\mathcal{T} = 10$ to 0.3. It can be seen that the harmonic content is reduced and kept close to the desired level. Nevertheless, it must be taken into account that the harmonic limitation is traded-off in the objective function by the softening variables λ_1 and λ_2 , which permits a transgression of the harmonic bounds depending on their weight \mathcal{W} . The FFT of the signal for both cases is provided in Fig. 11(b).

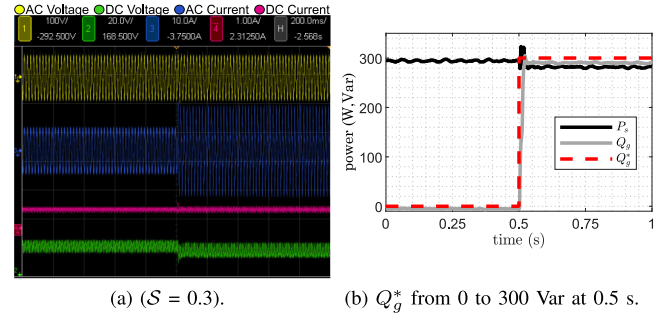


Fig. 12. Experimental results: reactive power reference change.

4) *Reactive Power Tracking*: The reactive power tracking performance is shown in Fig. 12. Note that Fig. 12b is obtained from the experimental data shown in Fig. 12(a). The reactive power reference changes from 0 to 300 Var at time 0.5 s. It is seen that the tracking is quite accurate despite the small error originated from the trade-off of the different elements of the objective function.

VII. CONCLUSION

This paper has introduced the design of an MPC energy regulator for VSCs. The two-level single-phase converter has been chosen to validate the MPC algorithm given the nonlinear relationship between the AC and DC sides of the converter. The algorithm has been designed to not only trade-off the different system states but to consider other system features such as efficiency, current harmonic injection or DC bus voltage ripple. However, it has been shown that the definition of a nonlinear MPC leads to a cumbersome computational burden, which is difficult to overcome in real-time. Therefore, a strategy to reduce the burden of the regulator has been discussed and the control structure has been designed to benefit from the characteristics of VSCs. Due to the slow energy dynamics of the system, the MPC has been defined considering an average model of the converter rather than its switching pattern, which is typically used in conventional FCS-MPC approaches. Thus, the predictive algorithm has been implemented at a reduced sampling frequency, since a faster inner regulator has also been added to keep the converter current stable under unexpected disturbances. The burden of the MPC has been further relaxed by applying an LTV linearisation. It has been shown that this strategy permitted to reduce the computational burden of the MPC by around two orders of magnitude compared to a nonlinear formulation. Additionally, the LTV approximation replicated the system dynamics accurately and the modelling error introduced did not significantly affect the performance of MPC. The computational complexity of the overall control structure has been shown to be sufficiently low for real-time implementation and the algorithm has been validated experimentally. The controller exhibited an adequate regulation of the system, improving the performance obtained with a conventional PI regulator. As a remark, it should be emphasised that the control algorithm can be easily adapted to other complex

$$\bar{I}_{lg} = \frac{1}{2(\omega^2 L^2 + R^2) \bar{V}_g} \left((-j\omega L + R) \sqrt{\bar{V}_g^4 + (4\omega L Q_g + 4P_s R) \bar{V}_g^2 - 4(\omega L P_s - Q_g R)^2 + 2\omega^2 L^2 P_s} \right. \\ \left. + \dots 2\omega L \left((jP_s - Q_g) R + \frac{j\bar{V}_g^2}{2} \right) - 2jQ_g R^2 - R\bar{V}_g^2 \right) \quad (29)$$

$$\bar{V}_l = \frac{1}{2\bar{V}_g} \left(2j\omega L P_s - 2jQ_g R + \bar{V}_g^2 + \sqrt{\bar{V}_g^4 + (4\omega L Q_g + 4P_s R) \bar{V}_g^2 - 4(\omega L P_s - Q_g R)^2} \right) \quad (30)$$

converter topologies by considering the corresponding system model.

APPENDIX A

The complex-domain analysis of the AC side of the system shown in Fig. 1(a) leads to the following expression:

$$\bar{V}_l - \bar{V}_g = (j\omega L + R) \bar{I}_{lg} \quad (27)$$

where j designates complex values. Besides, given a reactive power reference point Q_g to be tracked, the power at the converter is defined as

$$P_s + jQ_g = \bar{V}_l \bar{I}_{lg}^* \quad (28)$$

The steady-state trajectory of the AC side current and DC voltage, obtained from (27) and (28), are shown in (29) and (30) shown at the top of this page respectively.

The time-domain trajectories of the states are obtained from the complex analysis performed in (29)–(30) and are defined as

$$v_l(t) = \sqrt{2} |\bar{V}_l| \cos(\omega t + \angle \bar{V}_l) \quad (31)$$

$$i_{lg}(t) = \sqrt{2} |\bar{I}_{lg}| \cos(\omega t + \angle \bar{I}_{lg}) \quad (32)$$

where $|\bar{V}_l|$ and $|\bar{I}_{lg}|$ refer to the magnitude of (29)–(30) and $\angle \bar{V}_l$ and $\angle \bar{I}_{lg}$ to their angle. The energy exchanged at the AC grid must be equal to the one exchanged at the DC side, hence

$$e(t) = \int (P_s - v_l(t) i_{lg}(t)) dt \\ = P_s \cdot t - 2 |\bar{V}_l| |\bar{I}_{lg}| \left(\frac{\cos(\angle \bar{I}_{lg} - \angle \bar{V}_l) t}{2} \right. \\ \left. + \dots \frac{\sin(2\omega t + \angle \bar{I}_{lg} + \angle \bar{V}_l)}{4\omega} \right) + e_0. \quad (33)$$

Finally, the energy stored in the DC bus capacitor is

$$e_c(t) = \frac{C v_{dc}(t)^2}{2} \quad (34)$$

so that the DC bus voltage trajectory can be obtained as

$$v_{dc}(t) = \sqrt{\frac{2e_c(t)}{C}} = \sqrt{\frac{2e(t)}{C}}. \quad (35)$$

APPENDIX B

The linearisation (10) applied to the converter model (4) leads to

$$\frac{d}{dt} \begin{bmatrix} \tilde{v}_{dc}(t) \\ \tilde{i}_{lg}(t) \end{bmatrix} = \begin{bmatrix} \frac{1}{C} \left(\tilde{i}_s(t) - \frac{\tilde{v}_l(t) \tilde{i}_{lg}(t)}{\tilde{v}_{dc}(t)} \right) \\ \frac{1}{L} (\tilde{v}_l(t) - \tilde{v}_g(t) - R \tilde{i}_{lg}(t)) \end{bmatrix} \quad (36)$$

and

$$\frac{d}{dt} \begin{bmatrix} \delta v_{dc}(t) \\ \delta i_{lg}(t) \end{bmatrix} = \begin{bmatrix} \frac{\tilde{v}_l(t) \tilde{i}_{lg}(t)}{C \tilde{v}_{dc}^2(t)} & -\frac{\tilde{v}_l(t)}{C \tilde{v}_{dc}(t)} \\ 0 & -\frac{R}{L} \end{bmatrix} \begin{bmatrix} \delta v_{dc} \\ \delta i_{lg} \end{bmatrix} \\ + \begin{bmatrix} -\frac{\tilde{i}_{lg}(t)}{C \tilde{v}_{dc}(t)} \\ \frac{1}{L} \end{bmatrix} \begin{bmatrix} \delta v_l \\ \delta v_g \end{bmatrix} + \begin{bmatrix} \frac{1}{C} & 0 \\ 0 & -\frac{1}{L} \end{bmatrix} \begin{bmatrix} \delta i_s \\ \delta v_g \end{bmatrix}. \quad (37)$$

REFERENCES

- [1] S. Vazquez, J. Rodriguez, M. Rivera, L. G. Franquelo, and M. Norambuena, "Model predictive control for power converters and drives: Advances and trends," *IEEE Trans. Ind. Electron.*, vol. 64, no. 2, pp. 935–947, Feb. 2017.
- [2] T. Geyer, *Model Predictive Control of High Power Converters and Industrial Drives*. Hoboken, NJ, USA: Wiley, 2016.
- [3] M. Morari and J. H. Lee, "Model predictive control: Past, present and future," *Comput. Chem. Eng.*, vol. 23, no. 4–5, pp. 667–682, 1999, doi: [10.1016/S0098-1354\(98\)00301-9](https://doi.org/10.1016/S0098-1354(98)00301-9).
- [4] D. Mayne, "Control of constrained dynamic systems," *Eur. J. Control*, vol. 7, no. 2–3, pp. 87–99, Jan. 2001.
- [5] P. Karamanakos, E. Liegmann, T. Geyer, and R. Kennel, "Model predictive control of power electronic systems: Methods, results, and challenges," *IEEE Open J. Ind. Appl.*, vol. 1, pp. 95–114, 2020, doi: [10.1109/OJIA.2020.3020184](https://doi.org/10.1109/OJIA.2020.3020184).
- [6] J. Rodriguez *et al.*, "State-of-the-art of finite control set model predictive control in power electronics," *IEEE Trans. Ind. Informat.*, vol. 9, no. 2, pp. 1003–1016, May 2013.
- [7] S. Vazquez, P. Acuna, R. P. Aguilera, J. Pou, J. I. Leon, and L. G. Franquelo, "Dc-link voltage-balancing strategy based on optimal switching sequence model predictive control for single-phase H-NPC converters," *IEEE Trans. Ind. Electron.*, vol. 67, no. 9, pp. 7410–7420, Sep. 2020.
- [8] B. Stellato, T. Geyer, and P. J. Goulart, "High-speed finite control set model predictive control for power electronics," *IEEE Trans. Power Electron.*, vol. 32, no. 5, pp. 4007–4020, May 2017.
- [9] S. Almér, S. Mariéthoz, and M. Morari, "Sampled data model predictive control of a voltage source inverter for reduced harmonic distortion," *IEEE Trans. Control Syst. Technol.*, vol. 21, no. 5, pp. 1907–1915, Sep. 2013.
- [10] S. Almér, S. Mariéthoz, and M. Morari, "Dynamic phasor model predictive control of switched mode power converters," *IEEE Trans. Control Syst. Technol.*, vol. 23, no. 1, pp. 349–356, Jan. 2015.

- [11] S. Vazquez *et al.*, "Model predictive control for single-phase NPC converters based on optimal switching sequences," *IEEE Trans. Ind. Electron.*, vol. 63, no. 12, pp. 7533–7541, Dec. 2016.
- [12] S. Vazquez, A. Marquez, R. Aguilera, D. Quevedo, J. I. Leon, and L. G. Franquelo, "Predictive optimal switching sequence direct power control for grid-connected power converters," *IEEE Trans. Ind. Electron.*, vol. 62, no. 4, pp. 2010–2020, Apr. 2015.
- [13] P. Acuna, R. P. Aguilera, A. M. Y. M. Ghias, M. Rivera, C. R. Baier, and V. G. Agelidis, "Cascade-free model predictive control for single-phase grid-connected power converters," *IEEE Trans. Ind. Electron.*, vol. 64, no. 1, pp. 285–294, Jan. 2017.
- [14] D. Quevedo, R. Aguilera, M. Perez, P. Cortes, and R. Lizana, "Model predictive control of an AFE rectifier with dynamic references," *IEEE Trans. Power Electron.*, vol. 27, no. 7, pp. 3128–3136, Jul. 2012.
- [15] L. Cavanini, G. Cimini, G. Ippoliti, and A. Bemporad, "Model predictive control for pre-compensated voltage mode controlled DC-DC converters," *IET Control Theory Appl.*, vol. 11, no. 15, pp. 2514–2520, 2017.
- [16] L. Cavanini, G. Cimini, and G. Ippoliti, "Model predictive control for pre-compensated power converters: Application to current mode control," *J. Franklin Inst.*, vol. 356, no. 4, pp. 2015–2030, 2019.
- [17] J. M. Rodriguez-Bernuz and A. Junyent-Ferré, "Model predictive current reference calculation for single-phase VSCs," in *Proc. 18th Euro. Conf. Power Electron. Appl.*, 2016, pp. 1–10.
- [18] T. Geyer and D. E. Quevedo, "Multistep direct model predictive control for power electronics - Part 2: Analysis," in *Proc. IEEE Energy Convers. Congr. Expo.*, 2013, pp. 1162–1169, doi: [10.1109/ECCE.2013.6646836](https://doi.org/10.1109/ECCE.2013.6646836).
- [19] J. Rodriguez-Bernuz and A. Junyent-Ferré, "Operating region extension of a modular multilevel converter using model predictive control: A single-phase analysis," *IEEE Trans. Power Del.*, vol. 35, no. 1, pp. 171–182, Feb. 2020.
- [20] R. Erickson and D. Maksimovic, *Fundamentals of Power Electronics*, 2nd Ed. Berlin, Germany: Springer, 2001, doi: [10.1007/b100747](https://doi.org/10.1007/b100747).
- [21] V. Yaramasu and B. Wu, *Model Predictive Control of Wind Energy Conversion Systems*, Wiley, Dec. 2016. [Online]. Available: <https://www.wiley.com/en-us/Model+Predictive+Control+of+Wind+Energy+Conversion+Systems-p-9781118988589>.
- [22] H. Akagi, E. H. Watanabe, and M. Aredes, *Electric Power Definitions: Background*. Hoboken, NJ, USA: Wiley-IEEE Press, 2007, pp. 19–40.
- [23] P. Cortes, J. Rodriguez, D. E. Quevedo, and C. Silva, "Predictive current control strategy with imposed load current spectrum," *IEEE Trans. Power Electron.*, vol. 23, no. 2, pp. 612–618, Mar. 2008.
- [24] C. B. Moler, *Numerical Computing With Matlab. Soc. Ind. Appl. Math.*, 2004. [Online]. Available: <https://epubs.siam.org/doi/book/10.1137/1.9780898717952>
- [25] B. Stellato, G. Banjac, P. Goulart, A. Bemporad, and S. Boyd, "OSQP: An operator splitting solver for quadratic programs," *Math. Program. Comput.*, vol. 12, no. 4, pp. 637–672, 2020. [Online]. Available: <https://osqp.org/docs/citing/index.html>
- [26] The MathWorks Webpage, "Solve a quadratic programming problem using the KWIK algorithm," Aug. 2020. [Online]. Available: <https://uk.mathworks.com/help/mpc/ref/mpcqp solver.html>
- [27] S. Golestan, M. Monfared, F. D. Frejedo, and J. M. Guerrero, "Dynamics assessment of advanced single-phase PLL structures," *IEEE Trans. Ind. Electron.*, vol. 60, no. 6, pp. 2167–2177, Jun. 2013.
- [28] S. Skogestad and I. Postlethwaite, *Multivariable Feedback Control: Analysis and Design*. Hoboken, NJ, USA: Wiley, 1996.



Joan-Marc Rodriguez-Bernuz (Member, IEEE) received the bachelor's and master's degrees in energy engineering from the Barcelona College of Industrial Engineering, Polytechnic University of Catalonia, Barcelona, Spain, in 2013 and 2015, respectively and the Ph.D. degree in electrical engineering from Imperial College London, U.K., in 2019.

Since then, he has been a Research Associate with the Control and Power research group, Imperial College London. His research interests include control of power converters for renewable energy technologies, power transmission with specific focus on applied predictive controllers.



Ian McInerney (Member, IEEE) received the M.S. and B.S. degrees from Iowa State University, Ames, IA, USA, in 2017 and 2015, respectively.

Since 2017, he has been a PhD student at Imperial College London, U.K., in the High Performance Embedded and Distributed Systems (HiPEDS) Centre for Doctoral Training. His research interests include developing algorithms and digital architectures for the real-time implementation of control systems, with an emphasis on predictive control.



Adrià Junyent-Ferré (Senior Member, IEEE) received the Industrial Engineering degree from the School of Industrial Engineers of Barcelona, Polytechnic University of Catalonia (UPC), Spain, in 2007 and the Ph.D. degree in electrical engineering from UPC in 2011.

From 2006 to 2012, he was a Researcher with CITCEA-UPC and in 2012, a Lecturer with the Barcelona College of Industrial Engineering, Barcelona, Spain. In 2013, he joined the Department of Electrical and Electronic Engineering, Imperial

College London, U.K., where he is currently a Senior Lecturer. His research interests include power electronic converter applications for wind power generation, VSC-HVDC transmission, and low voltage distribution. He investigates how converters can be made resilient to network transients with minimal oversizing.



Eric C. Kerrigan (Senior Member, IEEE) received the B.Sc. degree in engineering from the University of Cape Town, South Africa, and the Ph.D. degree from the University of Cambridge, U.K.

His research interests include the design of efficient numerical methods and computing architectures for solving optimal control problems in real-time, with applications in the design of aerospace, renewable energy, and information systems.

He is the chair of the IFAC Technical Committee on Optimal Control, a Senior Editor of IEEE TRANSACTIONS ON CONTROL SYSTEMS TECHNOLOGY and an Associate Editor of IEEE TRANSACTIONS ON AUTOMATIC CONTROL and the *European Journal of Control*.